AD

TECHNICAL REPORT ARCCB-TR-02014

IN-SITU PHASE EVOLUTION STUDY IN MAGNETRON-SPUTTERED TANTALUM THIN FILMS

S. L. LEE
D. WINDOVER
T.-M. LU
M. AUDINO

OCTOBER 2002

US ARMY ARMAMENT RESEARCH,
DEVELOPMENT AND ENGINEERING CENTER
Close Combat Armaments Center
Benét Laboratories
Watervliet, NY 12189-4000

TACOM-ARDEC

APPROVED FOR PUBLIC RELEASE; DISTRIBUTION UNLIMITED

DISCLAIMER

The findings in this report are not to be construed as an official Department of the Army position unless so designated by other authorized documents.

The use of trade name(s) and/or manufacturer(s) does not constitute an official endorsement or approval.

DESTRUCTION NOTICE

For classified documents, follow the procedures in DoD 5200.22-M, Industrial Security Manual, Section II-19, or DoD 5200.1-R, Information Security Program Regulation, Chapter IX.

For unclassified, limited documents, destroy by any method that will prevent disclosure of contents or reconstruction of the document.

For unclassified, unlimited documents, destroy when the report is no longer needed. Do not return it to the originator.

REPORT DOCUMENTATION PAGE

Form Approved
OMB No. 0704-0188

1. AGENCY USE ONLY (*Leave Blank*)	2. REPORT DATE	3. REPORT TYPE AND DATES COVERED
	October 2002	Final

4. TITLE AND SUBTITLE
IN-SITU PHASE EVOLUTION STUDY IN MAGNETRON-SPUTTERED TANTALUM THIN FILMS

5. FUNDING NUMBERS
AMCMS No. 6111.02.H671.1

6. AUTHORS
S.L. Lee, D. Windover (RPI, Troy, NY), T.-M. Lu (RPI), and M. Audino

7. PERFORMING ORGANIZATION NAME(S) AND ADDRESS(ES)
U.S. Army ARDEC
Benet Laboratories, AMSTA-AR-CCB-O
Watervliet, NY 12189-4000

8. PERFORMING ORGANIZATION REPORT NUMBER
ARCCB-TR-02014

9. SPONSORING / MONITORING AGENCY NAME(S) AND ADDRESS(ES)
U.S. Army ARDEC
Close Combat Armaments Center
Picatinny Arsenal, NJ 07806-5000

10. SPONSORING / MONITORING AGENCY REPORT NUMBER

11. SUPPLEMENTARY NOTES
Presented at the International Conference on Metallurgical Coatings and Thin Films, San Diego, CA, 22-26 April 2002.
Published in *Metallurgical Coatings and Thin Films.*

12a. DISTRIBUTION / AVAILABILITY STATEMENT
Approved for public release; distribution unlimited.

12b. DISTRIBUTION CODE

13. ABSTRACT *(Maximum 200 words)*

The design and construction of a planar magnetron-sputter deposition system with a beryllium chamber was accomplished to perform *in-situ* x-ray diffraction growth study of refractory coatings. The deposition system was set on top of a laboratory θ-2θ x-ray diffractometer. A two-dimensional array detector was interfaced for observation of the Debye rings during growth. Integration along the 2θ and χ directions allows fast phase and texture determination. The system was built to study effects of sputter deposition parameters on the structural properties of tantalum on steel, silicon, and glass substrates without exposing the system to atmosphere pressure.

Two sputter depositions of tantalum films onto glass substrate in argon gas are reported here, one was deposited at 25-mm target-detector distance, 3.9 Pascal argon gas, and the other at 108-mm target-detector distance and 1.3 Pascal argon gas. The first film grew to 250-nm in 39 minutes at an average growth rate of 6.4-nm/minute. It consisted of 45-nm of interface layer, which showed no crystalline structure, and was most likely amorphous film. It was followed by 15-nm growth of β-tantalum, and then followed by 190-nm growth of α-tantalum. From the full-width half maximum of the χ-plot, it was determined that the β-tantalum region was <002> textured, and the α-tantalum region was <110> textured, and grew more textured with deposition time. The second film grew to 36-nm in 22 minutes at an average growth rate of 1.6-nm/minute. It consisted of 31-nm of layer, which showed no crystalline structure, and was most likely amorphous film. It was followed by 5-nm of surface layer of β- and α-tantalum. *Ex-situ* grazing incidence x-ray diffraction performed on the film surface confirmed the *in-situ* results. *Ex-situ* pole figure analysis showed <110> fiber texture in α-tantalum, and highly <002> texture in β-tantalum.

14. SUBJECT TERMS
In-Situ Characterization, Magnetron Sputtering, Real-Time X-Ray Diffraction, Tantalum, Two-Dimensional Detector

15. NUMBER OF PAGES
18

16. PRICE CODE

17. SECURITY CLASSIFICATION OF REPORT	18. SECURITY CLASSIFICATION OF THIS PAGE	19. SECURITY CLASSIFICATION OF ABSTRACT	20. LIMITATION OF ABSTRACT
UNCLASSIFIED	UNCLASSIFIED	UNCLASSIFIED	UL

TABLE OF CONTENTS

TABLES

LIST OF ILLUSTRATIONS

ACKNOWLEDGEMENTS

Funding supports are greatly appreciated for this work, including U.S. Army Environmental Quality Basic Research and Development Program (EQBRD), and the New York Focus Center, a joint partner in the national Interconnect Focus Center (IFC), under Microelectronics Advanced Research Corp. (MARCO)/Defense Advanced Research Projects Agency (DARPA).

INTRODUCTION

The ability to perform a real-time growth study of thin films is important in the development of quality refractory coatings for high-temperature tri-service (armed forces) wear and erosion applications. Properties of coatings at the coating-substrate interface and in the coating bulk control the coating performance. However, quantitative tools for phase and structural characterization of thin films during the early stages of deposition are limited. Nondestructive *in-situ* x-ray analysis allows easy changing and monitoring of sputtering parameters without exposing the system to external atmospheric contamination. This provides a direct correlation between deposition parameters and thin-film properties and the determination of the most favorable conditions for the growth of quality films. Furthermore, a two-dimensional position-sensitive array detector facilitates fast real-time monitoring of phase and texture for growing thin films.

Environmentally friendly tantalum has many diversified applications. It is a potential material to replace chromium for the protection of gun bores against high-temperature wear and erosion (refs 1,2). It is also a diffusion barrier material to prevent copper diffusion for the electronics industry (refs 3-6). Tantalum forms in two phases: an α-phase (body-centered-cubic, Space group Im-3m), which is soft, ductile, and chemically resistant to aggressive hot propellant gases; and a β-phase (tetragonal, Space group P42/mnm), which is hard, brittle, and thermally/mechanically unstable (refs 7-9). A face-centered- cubic phase (Space group Fm-3m) has been reported, but its existence has not been confirmed (ref 8). The α-phase is favored over the β-phase for high-temperature wear and erosion applications because of its superior physical properties, and its excellent performance in high-temperature cyclic firing tests (refs 9-11). The α-phase is also favored for semiconductor interconnects due to its high-temperature behavior, higher electrical conductivity, and slightly higher density (refs 3-6, 8). Sputtering conditions, which favor α-tantalum nucleation and growth, are of prime importance in the development of quality coatings (refs 9-15).

The construction of *in-situ* x-ray diffraction instrumentation using an Inel, one-dimensional position sensitive array detector has been reported (refs 16-18). The instrument was applied to study impurity incorporation, deposition kinetics, and microstructure evolution in sputtered tantalum thin films (refs 18,19). However, the sputtering depositions at 12-nm/minute as a function of argon pressure resulted in all β-tantalum films.

In this work, a detachable DC planar magnetron-sputtering deposition system was constructed on top of a laboratory θ-2θ x-ray diffractometer with Bragg-Brentano geometry to study sputtering deposition of tantalum in real-time. A two-dimensional array detector was interfaced to the system to provide fast phase and texture information from integration of the Debye rings. Two sputter depositions of tantalum films in argon gas onto glass slides are reported herein. One was deposited at 25-mm target-detector distance, 3.9 Pascal argon gas, and the other at 108-mm target-detector distance and 1.3 Pascal argon gas. Future depositions on steel and silicon substrates at various sputter parameters are planned.

IN-SITU SPUTTERING DEPOSITION SYSTEM

Figure 1a shows a schematic side view of the x-ray source, optics, sample specimen location, and the two-dimensional detector, relative to the sputter deposition vacuum system, which is perpendicular to the page. Figure 1b shows a photo of the *in-situ* sputtering deposition system in operation, with corresponding parts in the schematics as follows:

- X-ray source and optics (A)
- Goniometer (B)
- Sputter vacuum system (C)
- Beryllium chamber (D)
- Two-dimensional array detector (E)

A detailed description of the design and construction of the *in-situ* sputter deposition system is given in a separate document (ref 20). The major system components include:

- A stainless steel sputter chamber, 64-mm in diameter by 280-mm long, constructed by Brush Wellman. The beryllium (99% pure) window section was 64-mm in diameter by 75-mm long, and 0.5-mm thick. Chamber end plates for gas and water inlets and sputter head feed-through were made of stainless steel and were constructed by Rensselaer Polytechnic Institute.

- A 25.4-mm diameter sputter head and a shutter assembly, constructed by Angstrom Sciences. It used a neodymium iron encapsulated magnetron for plasma enhancement. The shutter acts as a catcher for sputter cleaning of the target. There was no collimator used. The target was water-cooled, but not the substrate.

- An MKS cluster controller and mass flow controllers, Alcatel turbo-molecular pump and roughing pump, valves and piping, etc., were assembled for vacuum control/gas handling. The system pressure after a one-day pump-down was ~1.3 x 10^{-4} Pascal (~1 x 10^{-6} Torr); after nine days, pump-down was 1.3 x 10^{-5} Pascal (~1 x 10^{-7} Torr).

- A Scintag four-axis diffractometer, with a conventional ~2Kwatt x-ray source, pinhole and collimator, adjustable diffractometer circle (current radius set to 286-mm) was used as framework for the sputtering system.

- A two-dimensional Bruker position-sensitive array detector, with 1024 x 1024 wire elements and active face diameter of 115-mm, was mounted on the diffractometer 2θ-axis by a dovetail-riser for x-ray diffraction measurements. The specimen-to-detector distance used in this work was 150-mm. (Note: the array detector does not use Bragg-Brentano focusing geometry.)

- An alternative Peltier-cooled Si(Li) detector, mounted on the diffractometer 2θ-axis, with associated single-channel analyzer for energy discrimination, allowed *ex-situ* x-ray diffraction and pole figure analysis. It also allowed *in-situ* and *ex-situ* x-ray reflectivity film thickness measurements (ref 20).

The magnetron system provides operating power between 10 and 150 watts and gas pressure of 0.6 to 13 Pascal (5 to 100 mTorr). To protect the beryllium window from being contaminated with the sputtered material, an inner lining of high vacuum compatible Kapton® was wrapped around the longitudinal axis of the chamber during operation.

EXPERIMENTAL METHODS

Table 1 lists the system parameters used for the two sputter depositions:

- 10 watts power
- Floating bias
- 99.999% argon gas
- 25.4-mm diameter 99.95% pure tantalum target

Table 1 Experimental Parameters Used in the *In-Situ* Sputter Deposition of Tantalum Films

Film/ Substrate Sample	Target/ Substrate Distance (mm)	Shutter Time (min.)	Argon Pressure (Pascal)	Deposition Time (min.)	Thickness (nm)	Data Frames (#)	Growth Surface Phase Texture
Ta/Glass (010531)	25	0	3.9	40	250 ±50[a]	22	Mostly Crystalline Thin β-Ta, Thicker α-Ta <002> β, <110> α
Ta/Glass (010907)	108	2	1.3	22	36 ±3.6[b]	14	Mostly Noncrystalline Thin β-Ta, Thin α-Ta <002> β, <110> α

[a] Scanning electron microscopy cross-section measurement error.
[b] Wavelength dispersive x-ray fluorescence/x-ray reflectivity measurement error.

The substrate was American Scientific Products microfloat glass slide with low surface roughness to facilitate x-ray reflectivity thickness determination (ref 20). The 010531-deposition was made at 25-mm target-substrate distance, 3.9 Pascal argon pressure, before the shutter mechanism was installed. Installation of the shutter mechanism, designed by Angstrom Sciences, limited target-substrate distance to >50-mm. The 010907-deposition was made at 108-mm and 1.3 Pascal, using a two-minute shutter closed time to clean the target. No bake-out of the chamber was performed for the depositions. Both as-deposited films showed mirror-like surface shine characteristic of metallic tantalum coatings.

Copper K_α radiation at 40 mA, 45 kV was used for *in-situ* and *ex-situ* x-ray diffraction analyses. For the *in-situ* analysis, the two-dimensional detector was located at 150-mm from the specimen at $2\theta = 50°$, $\omega = 26°$. Debye ring data frames were obtained using one-minute accumulation time, at one-minute intervals for the entire duration of the deposition. A frame simultaneously collected data from 28° to 62° in 2θ, and -15° to 15° χ angles. Total film thickness was obtained using several techniques. A JEOL JSM-6335 field emission scanning electron microscope was used to image the cross-section thickness of the film. X-ray reflectivity provided thin-film thickness measurements. Comparison of tantalum L_α and L_β fluorescence intensities on a Siemens SRS 3000 wavelength dispersive x-ray fluorescence system, calibrated

using standards from Rutherford backscattering spectroscopy, also provided film thickness (ref 20). Thickness values for the noncrystalline, β-, and α-tantalum layers were then deduced from deposition time and analysis of the Debye rings.

RESULTS

Figure 2 gives five data frames showing predeposition and the progressive growth of Debye rings for specimen 010531. Similar predeposition and growth Debye rings for specimen 010907 are not shown. In the figure, body-centered-cubic α(110) and tetragonal β(002) reflections were observed at 38.47° and 33.69° 2θ, on the right of the frames. Two strong beryllium lines, Be(100) and Be(002), were observed on the left of the frames. The beryllium lines showed large grain effects (discontinuous intensities in the Debye Rings). Beryllium 2θ positions were displaced due to the location of the beryllium window. A faint line at 43° 2θ was attributed to α-tantalum formation on the Kapton® window protector used to shield the chamber surfaces.

Progressive changes of 22 data frames from 010531, and 14 frames from 010907, were carefully examined. For specimen 010531, the first six frames showed no crystalline structure, suggesting the film was most likely amorphous, following the amorphous nature of the substrate. This is subjected to further investigation. The growth was followed by β-tantalum (002) reflection in frames 7 and 8. Growth of moderately textured (110) α-tantalum was observed in frames 8 through 22, which prohibited further growth of β-tantalum. For specimen 010907, 12 of the 14 data frames showed no crystalline structure, suggesting the film was likely amorphous; only the last two frames showed almost simultaneous growth of β-tantalum (002) and α-tantalum (110).

Figure 3a shows the 2θ plot of data extracted from the growth Debye rings for specimen 010531, using an integration window of 2θ (28° to 62°), and χ (-12° to +11°). This figure depicts predeposition and β-tantalum (002) and α-tantalum (110) intensities at 11, 20, 31, and 39 minutes. Figure 3b shows the phase evolution of the film as time progressed, plotted on the same scale. This figure depicts the initial deposition of an amorphous layer, following growth of tetragonal β-tantalum, following the growth of α-tantalum.

Figure 4a shows x-ray intensity versus deposition time, showing 7-minutes/45-nm noncrystalline layer, followed by a 2-minute/15-nm β-tantalum layer, followed by 30-minute/190-nm α-tantalum layer. Figure 4b shows a scanning electron microscope image of the cross-section of a fractured surface of 010531 used for a total film thickness estimate. This total thickness translates to growth phase analysis of the 45-nm noncrystalline layer, 15-nm β-tantalum layer, and 190-nm α-tantalum layer in the specimen.

Figure 5 shows the χ-plots of α-tantalum (110) reflection, revealing the texture evolution of the film. The full-width half maximum at a 20-minute deposition was 35°, and at a 39-minute deposition, it was 23°, indicating the growth of more <110> textured α-tantalum layer as time progressed. For specimen 010907, these data translate into a 20-minute (~31-nm) growth of noncrystalline layer, followed by β- and α-tantalum growth for 3 minutes (~5-nm).

Figure 6 shows *ex-situ* conventional x-ray diffraction versus grazing incidence x-ray diffraction at $\omega = 5°$ for specimen 010531, normalized to the same scale. The data agree with the *in-situ* results, showing β-tantalum (002) and α-tantalum (110) contents on weak amorphous background from glass substrate and tantalum deposition. Surface and subsurface phase contents did not change significantly.

Figure 7a shows α(110) and Figure 7b shows α(200) pole figures for specimen 010531, obtained on the Scintag using $5° \chi$ x $5° \phi$ step collections. The intense center peak in Figure 7a, and the ring at 45° χ in Figure 7b, showed <110> fiber texture in α-tantalum. The fiber axis was at $\chi = 3°$, indicating the film may be growing at a small tilt angle relative to the normal of the film surface. This can be caused by the position of the sputter target relative to the substrate. The pole figure for β(002), not shown here, gave a strong central peak, indicating strong (002) texture in β-tantalum.

Figure 8 shows *ex-situ* conventional x-ray diffraction compared with grazing incidence x-ray diffraction at $\omega = 5°$ for specimen 010907. The bottom graph shows β(002) and α(110) on a very high amorphous background, in agreement with the *in-situ* results. A grazing incident scan amplifies the surface features for thin films. The grazing incidence data showed a reduction of the amorphous background, and higher intensity (110) α-tantalum compared to (002) β-tantalum. The surface layer thus has higher α-phase content compared to the subsurface layer in this specimen.

DISCUSSION

The *in-situ* sputtering system was designed and constructed to allow real-time observation of early stages of thin-film deposition, important for the development of thicker coatings. The two-dimensional array detector is ideal for a real-time growth study because of the fast acquisition speed compared to the growth rate of the film. Since integrating intensity over the χ range of a Debye ring was used, smaller sample times provided an averaged x-ray intensity for phase determination in textured film real-time. Analyzing this χ dimension separately (integrating small regions of 2θ provided fast texture information.

The x-ray penetration depth (1/e of original intensity) for copper K_α is ~1 μm for typical x-ray incident and exit angles of 26° and 50°, assuming an x-ray absorption coefficient of 161.5 cm^2/gm. An x-ray is expected to penetrate the entire thickness of the films under study in this work. However, contributions from surface layers dominate over subsurface layers. Also, we studied the progressive changes of Debye ring intensity for the growth surfaces by comparing results of consecutive runs. Grazing incidence *in-situ* work could also be performed, which would enhance surface and reduce the substrate effects. This is difficult due to space restrictions and lower overall peak intensities (further loss of Bragg-Brentano focusing) that are expected.

High impurities, such as H_2O, O_2, N_2, and C, are expected in the present system, since the system walls did not undergo bake-out and only minimum reverse sputter clean of the target was performed. Also, degassing of chamber walls and Kapton® protector are expected. At 1.3 to 4 Pascal (10 to 30 mTorr) argon pressure, tantalum neutrals are mostly thermal, after undergoing collisions before reaching the substrate. The current observation showed the growth of a mostly noncrystalline film at greater target-substrate distance for the second film. Longer deposition

times are required to grow equal thickness films. At the greater distance, the slower deposition rate allows more time for impurities, such as oxygen, to be incorporated into the film.

The growth of α- and β-tantalum is of great interest to the success of wear and erosion coatings. We observed β-tantalum nucleation and almost simultaneous growth of β-tantalum and α-tantalum, followed by continued growth of only α-tantalum. In other *in-situ* studies of tantalum (refs 18,19), only β-tantalum nucleation and growth were observed. Growth of an interface layer of β-tantalum before growth of α-tantalum is common, but simultaneous growth of α- and β-tantalum, and growth of α-tantalum at the interface and then β-tantalum have also been observed (refs 9-15). Most analyses of the crystalline phase were based on more qualitative photomicrograph and hardness data. Several factors have been suggested to promote nucleation and growth of α-tantalum (refs 12-15). Since phase formation is strongly dependent on deposition parameters, such as gas pressure, gas species, bias, substrate temperature, and film-substrate interface layer, future parametric studies on steel and silicon substrates are planned.

REFERENCES

1. Cox, J.F., and McClanahan, E.D., in: *Proceedings of Tri-Service Gun Tube Wear and Erosion Symposium*, 1982, p. 277.

2. Vasilakis, J., Strategic Environmental Research and Development Program (SERDP)- Tri-Service Green Gun Barrel Project, Year-End Report, Benet Laboratories, Watervliet, NY, 2000.

3. Jaeger, R.C., *Introduction to Microelectronics Fabrication*, Addison-Wesley, NY, 1993.

4. Holloway, K., and Fryer, P., *Applied Physics Letters*, Vol. 57, No. 17, 1990, p. 1736.

5. Roy, R.A., Catania, P., Saenger, K.L., Cuomo, J.J., and Lossy, R.L., *Journal of Vacuum Science and Technology B*, Vol. 11, No. 5, 1993, p. 1921.

6. Catania, Philippe, Roy, Ronnen A., and Cuomo, Jerome J., *Journal of Applied Physics*, Vol. 74, No. 2, 1993, p. 1008.

7. International Center for Diffraction Data, (ICDD), Newton Square, PA, 2001.

8. Baker, P.N., *Thin Solid Films*, Vol. 14, 1972, p. 3.

9. Lee, S.L., and Windover, D., *Surface and Coatings Technology*, Vol. 108-109, 1998, p. 65.

10. Lee, S.L., Cipollo, M., Windover, D., and Rickard, C., *Surface and Coatings Technology*, Vol. 120-121, 1999, p. 44.

11. Lee, S.L., Windover, D., Audino, M., Matson, D.W., and McClanahan, E.D., *Surface Coatings and Technology*, Vol. 149, 2002, p. 62.

12. Matson, D.W., Merz, M.D., and McClanahan, E.D., *Journal of Vacuum Science and Technology A*, Vol. 10, No. 4, 1992, p. 1791.

13. Matson, D.W., McClanahan, E.D., Rice, J.P., Lee, S.L., and Windover, D., *Surface and Coatings Technology*, Vol. 133-134, 2000, p. 411.

14. Matson, D.W., McClanahan, E.D., Lee, S.L., and Windover, D., *Surface and Coatings Technology*, Vol. 147-148, 2001, p. 344.

15. Ino, K., Shinohara, T., Ushikai, T., and Ohmi, T., *Journal of Vacuum Science and Technology A*, Vol. 15, 1997, p. 2627.

16. Angilello, J., Thompson, R.D., and Tu, K.N., *Journal of Applied Crystallography*, Vol. 22, 1989, p. 523.

17. *Inel Electronic Instrumentation Manual*, Inel, Inc., Stratham, NH, 1996.

18. Whitacre, J.F., Ph.D. Dissertation, University of Michigan, 2000.

19. Whitacre, J.F., Yalisove, S.M., and Bilello, J.C., *Materials Research Society Proceedings*, Vol. 562, 1999, p. 141.

20. Windover, D., Ph.D. Dissertation, Rensselaer Polytechnic Institute, Troy, NY, 2002.

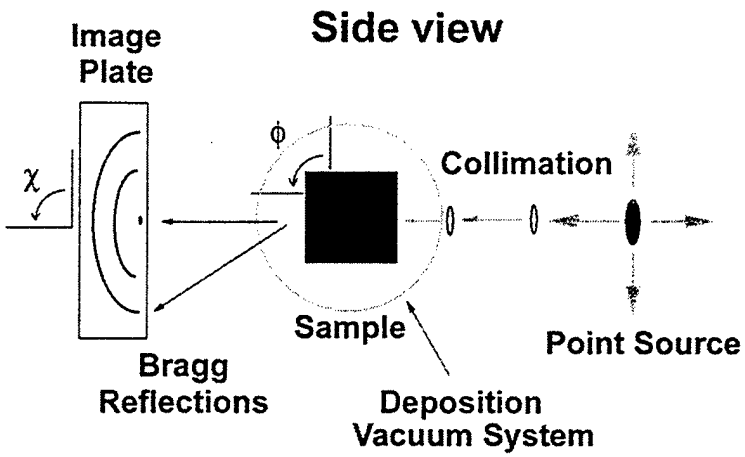

Figure 1a. Schematic side view of the x-ray source and collimating optics on the right, two-dimensional array detector on the left, and sample specimen in the middle.

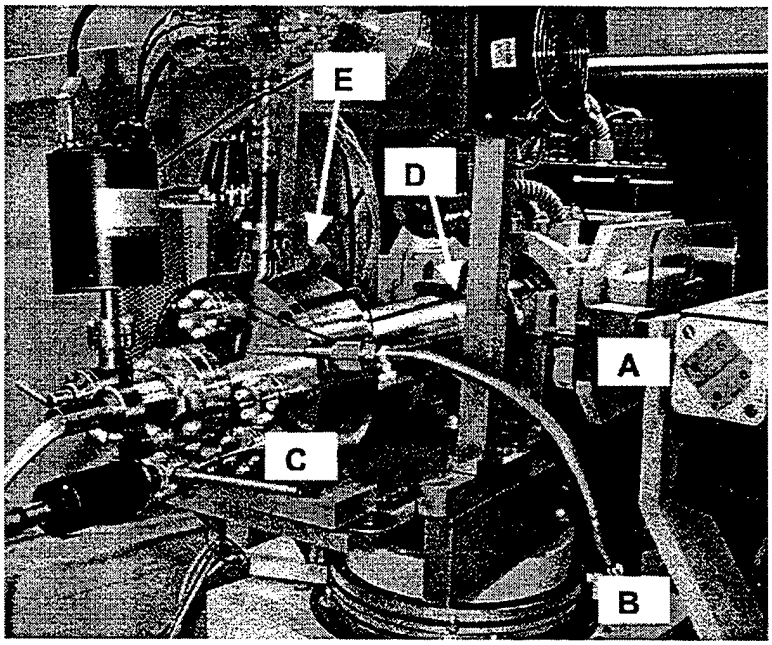

Figure 1b. Magnetron-sputtering system on top of x-ray diffractometer for *in-situ* x-ray diffraction characterization. The figure shows x-ray tube and collimation optics (A), goniometer (B), sputter head and vacuum system (C), beryllium chamber (D), and the two-dimensional array detector (E, behind chamber).

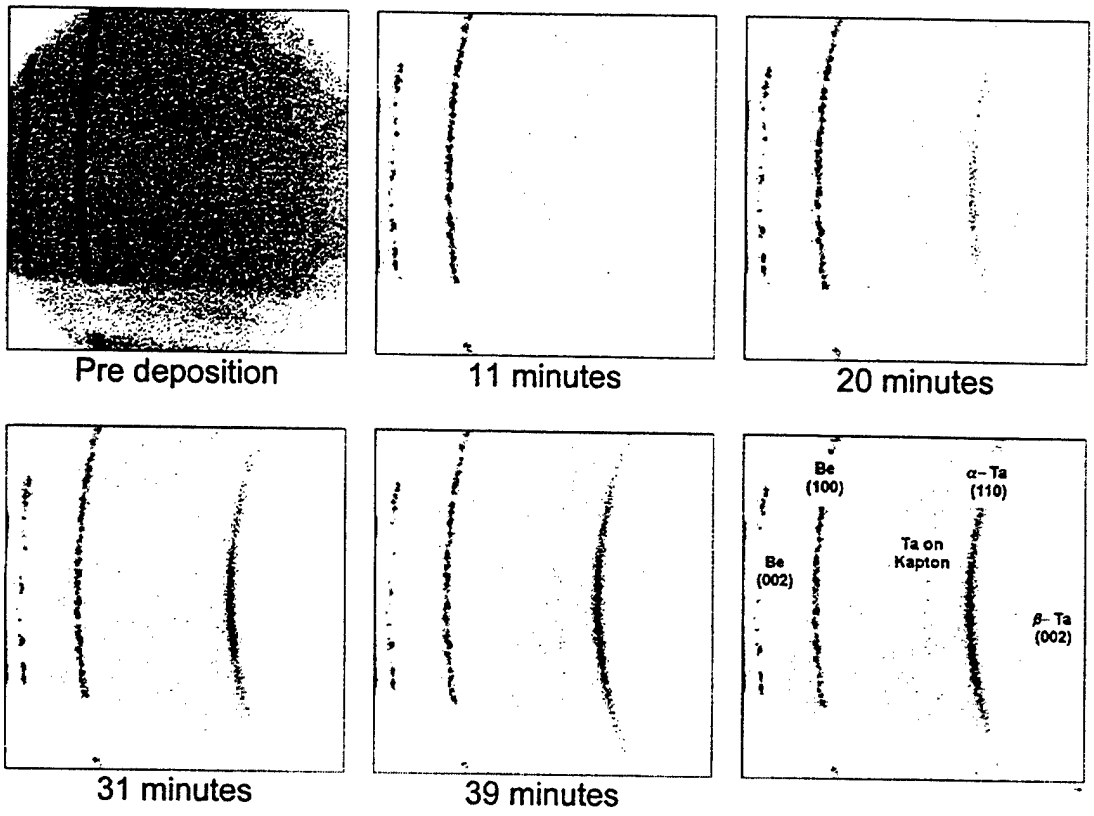

Figure 2. Selected data frames for *in-situ* analysis of specimen 010531, showing predeposition and progressive growth at 11, 20, 31, and 39 minutes.

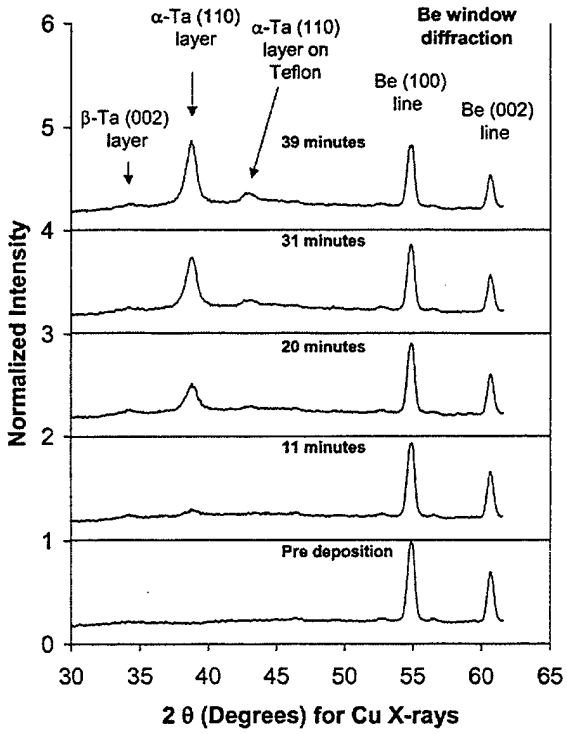

Figure 3a. Raw digital data extracted from Debye rings using integration in the χ direction to obtain 2θ data for specimen 010531.

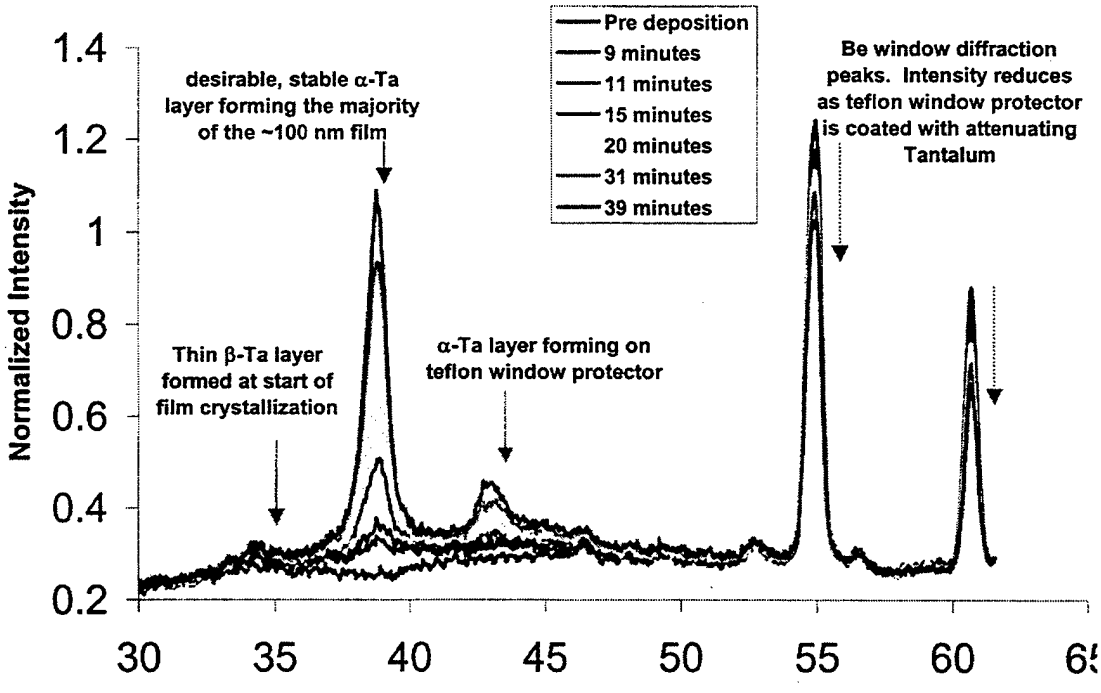

Figure 3b. Raw digital data showing the phase evolution of tantalum film for specimen 010531.

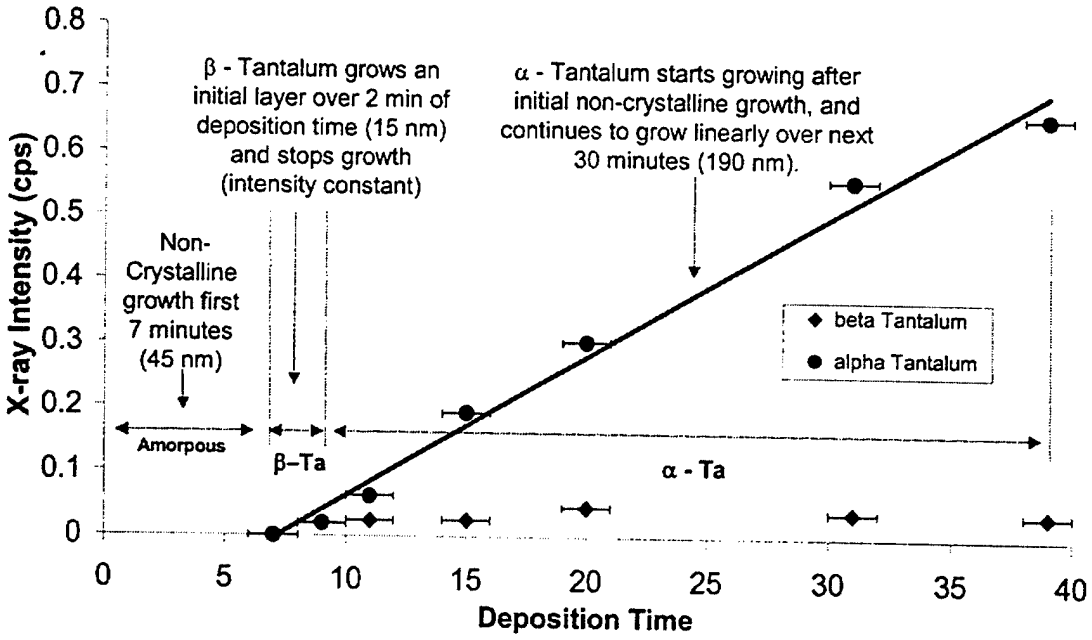

Figure 4a. Growth curve showing the analysis of phase evolution in specimen 010531

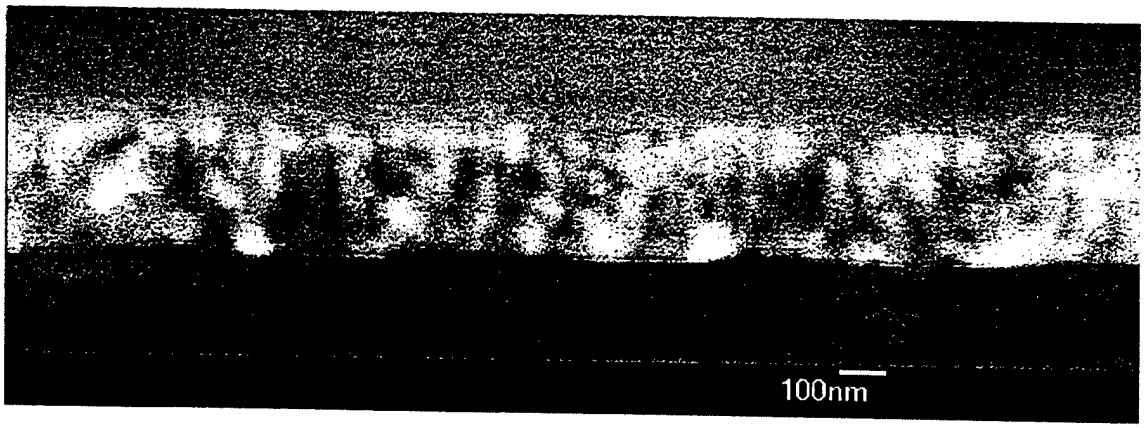

Figure 4b. Scanning electron measurement of total film thickness for specimen 010531.

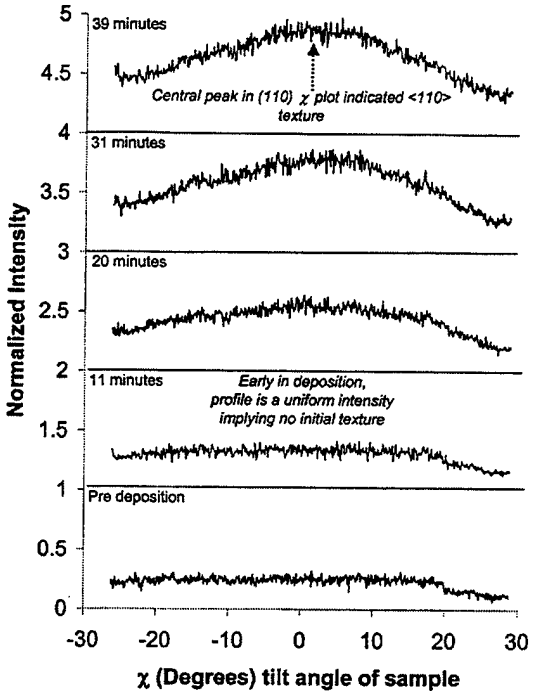

Figure 5. Texture evolution in specimen 010531, showing changes in the χ-plots using 2θ integration of data extracted from Figure 2.

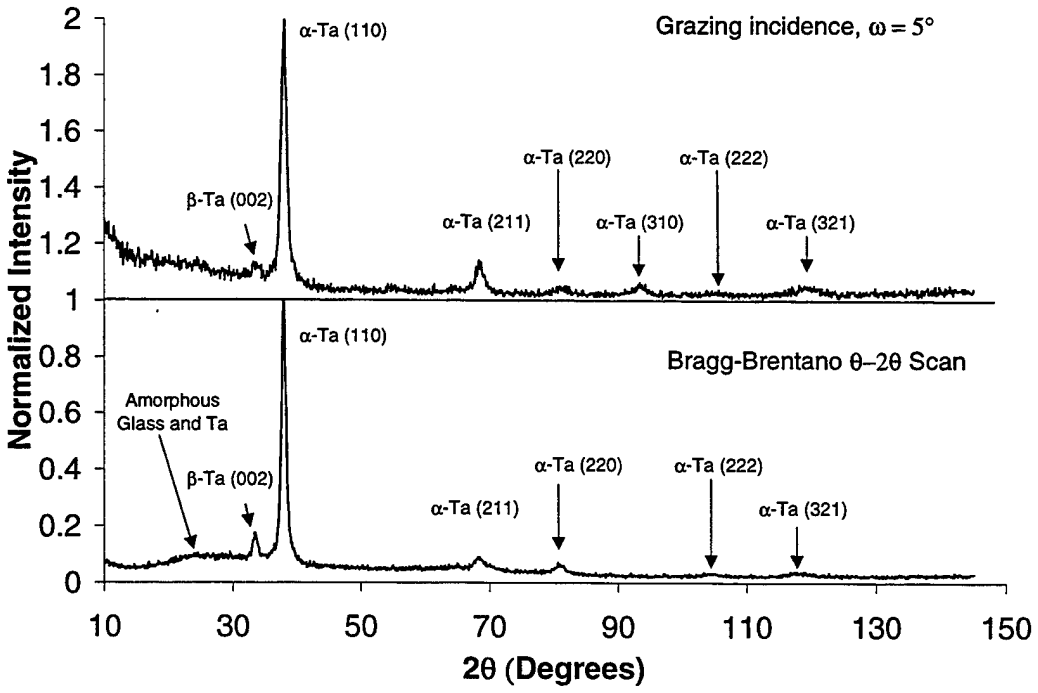

Figure 6. *Ex-situ* conventional x-ray diffraction (bottom) and grazing incidence x-ray diffraction (top) for specimen 010531.

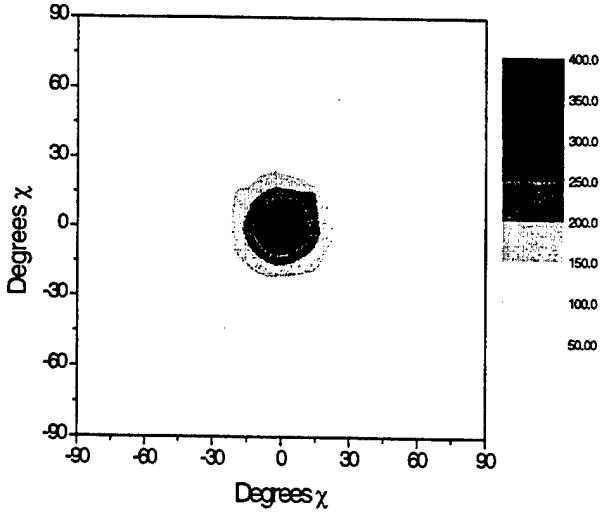

Figure 7a. Results of (110) pole figure analysis with strong central peak at ~0° χ.

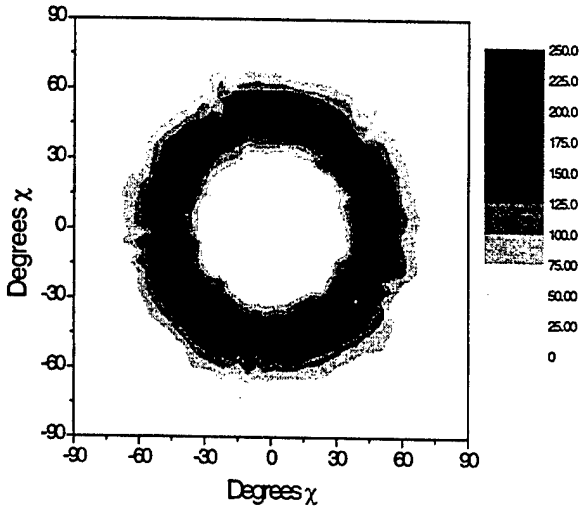

Figure 7b. Results of (200) pole figure analysis with ring at 45° χ.

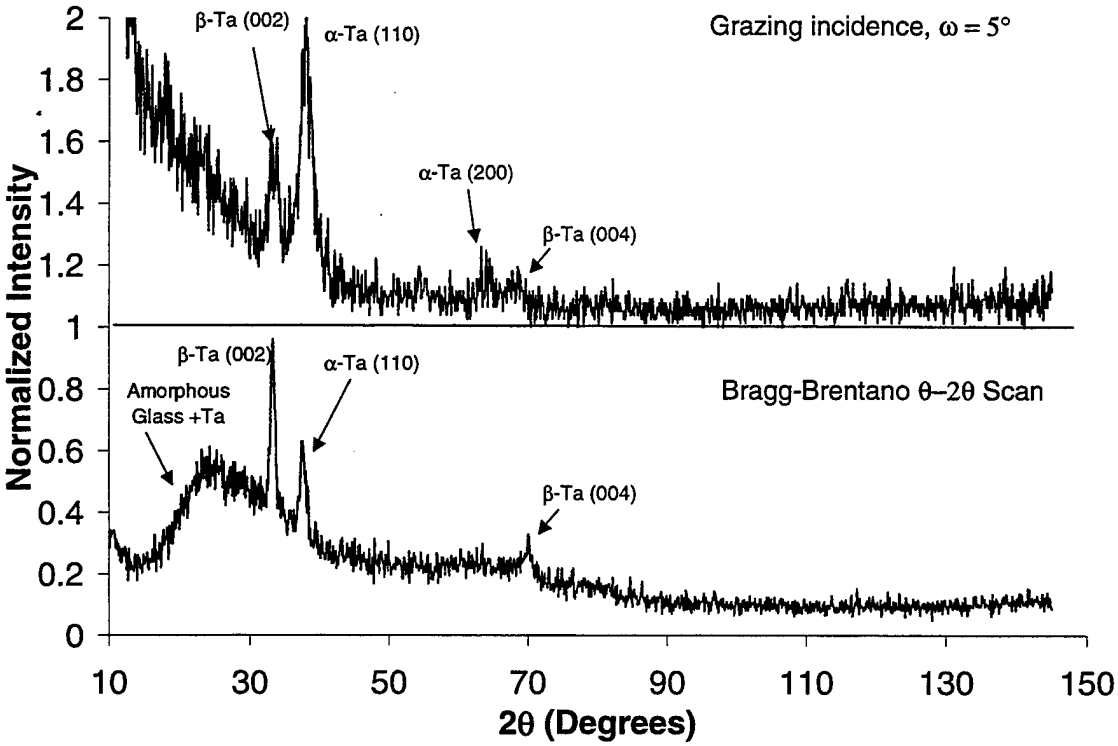

Figure 8. *Ex-situ* conventional x-ray diffraction (bottom) and grazing incidence x-ray diffraction (top) for specimen 010907.

TECHNICAL REPORT INTERNAL DISTRIBUTION LIST

	NO. OF COPIES
TECHNICAL LIBRARY ATTN: AMSTA-AR-CCB-O	5
TECHNICAL PUBLICATIONS & EDITING SECTION ATTN: AMSTA-AR-CCB-O	3
OPERATIONS DIRECTORATE ATTN: SIOWV-ODP-P	1
DIRECTOR, PROCUREMENT & CONTRACTING DIRECTORATE ATTN: SIOWV-PP	1
DIRECTOR, PRODUCT ASSURANCE & TEST DIRECTORATE ATTN: SIOWV-QA	1

NOTE: PLEASE NOTIFY DIRECTOR, BENÉT LABORATORIES, ATTN: AMSTA-AR-CCB-O OF ADDRESS CHANGES.

TECHNICAL REPORT EXTERNAL DISTRIBUTION LIST

	NO. OF COPIES
DEFENSE TECHNICAL INFO CENTER ATTN: DTIC-OCA (ACQUISITIONS) 8725 JOHN J. KINGMAN ROAD STE 0944 FT. BELVOIR, VA 22060-6218	2
COMMANDER U.S. ARMY ARDEC ATTN: AMSTA-AR-WEE, BLDG. 3022 AMSTA-AR-AET-O, BLDG. 183 AMSTA-AR-FSA, BLDG. 61 AMSTA-AR-FSX AMSTA-AR-FSA-M, BLDG. 61 SO AMSTA-AR-WEL-TL, BLDG. 59 PICATINNY ARSENAL, NJ 07806-5000	 1 1 1 1 1 2
DIRECTOR U.S. ARMY RESEARCH LABORATORY ATTN: AMSRL-DD-T, BLDG. 305 ABERDEEN PROVING GROUND, MD 21005-5066	 1
DIRECTOR U.S. ARMY RESEARCH LABORATORY ATTN: AMSRL-WM-MB (DR. B. BURNS) ABERDEEN PROVING GROUND, MD 21005-5066	 1
COMMANDER U.S. ARMY RESEARCH OFFICE ATTN: TECHNICAL LIBRARIAN P.O. BOX 12211 4300 S. MIAMI BOULEVARD RESEARCH TRIANGLE PARK, NC 27709-2211	 1

	NO. OF COPIES
COMMANDER ROCK ISLAND ARSENAL ATTN: SIORI-SEM-L ROCK ISLAND, IL 61299-5001	 1
COMMANDER U.S. ARMY TANK-AUTMV R&D COMMAND ATTN: AMSTA-DDL (TECH LIBRARY) WARREN, MI 48397-5000	 1
COMMANDER U.S. MILITARY ACADEMY ATTN: DEPT OF CIVIL & MECH ENGR WEST POINT, NY 10966-1792	 1
U.S. ARMY AVIATION AND MISSILE COM REDSTONE SCIENTIFIC INFO CENTER ATTN: AMSAM-RD-OB-R (DOCUMENTS) REDSTONE ARSENAL, AL 35898-5000	 2
COMMANDER U.S. ARMY FOREIGN SCI & TECH CENTER ATTN: DRXST-SD 220 7TH STREET, N.E. CHARLOTTESVILLE, VA 22901	 1

NOTE: PLEASE NOTIFY COMMANDER, ARMAMENT RESEARCH, DEVELOPMENT, AND ENGINEERING CENTER, BENÉT LABORATORIES, CCAC, U.S. ARMY TANK-AUTOMOTIVE AND ARMAMENTS COMMAND, AMSTA-AR-CCB-O, WATERVLIET, NY 12189-4050 OF ADDRESS CHANGES.